Electronic structure of monolayer 1T'-$MoTe_2$ grown by molecular beam epitaxy

Shujie Tang[1,2,3,4,5], Chaofan Zhang[1,2,6,7], Chunjing Jia[1, 2], Hyejin Ryu[3,8], Choongyu Hwang[9], Makoto Hashimoto[10], Donghui Lu[10], Zhi Liu[4,5], Thomas P. Devereaux[1, 2], Zhi-Xun Shen[1,2*], Sung-Kwan Mo[3*]

[1]*Stanford Institute for Materials and Energy Sciences, SLAC National Accelerator Laboratory, 2575 Sand Hill Road, Menlo Park, California 94025, USA*

[2]*Geballe Laboratory for Advanced Materials, Departments of Physics and Applied Physics, Stanford University, Stanford, California 94305, USA*

[3]*Advanced Light Source, Lawrence Berkeley National Laboratory, Berkeley, California 94720, USA*

[4]*State Key Laboratory of Functional Materials for Informatics, Shanghai Institute of Microsystem and Information Technology, Chinese Academy of Sciences, Shanghai 200050, China*

[5]*School of Physical Science and Technology, Shanghai Tech University, Shanghai 200031, China*

[6]*College of Optoelectronic Science and Engineering, National University of Defense Technology, Changsha 410073, China*

[7]*Interdisciplinary Center of Quantum Information, National University of Defense Technology, Changsha 410073, China*

[8]*Max Planck-POSTECH/Hsinchu Center for Complex Phase Materials, Max Plank POSTECH/Korea Research Initiative (MPK), Gyeongbuk 37673, Korea*

[9]*Department of Physics, Pusan National University, Busan 46241, Korea*

[10]*Stanford Synchrotron Radiation Lightsource, SLAC National Accelerator Laboratory, 2575 Sand Hill Road, Menlo Park, California 94025, USA*

**E-mail: zxshen@stanford.edu, skmo@lbl.gov*

Abstract

Monolayer transition metal dichalcogenides (TMDCs) in 1T' structural phase have drawn a great deal of attention due to the prediction of quantum spin Hall insulator states. The band inversion and the concomitant changes in the band topology induced by the structural distortion from 1T to 1T' phases are well established. However, the band gap opening due to the strong spin-orbit coupling (SOC) is only verified for 1T'-WTe_2 recently and still debated for other TMDCs. Here we report a successful growth of high-quality monolayer 1T'-$MoTe_2$ on bilayer graphene substrate through molecular beam epitaxy. Using in-situ angle-resolved photoemission spectroscopy (ARPES), we have investigated the low-energy electronic structure and Fermi surface topology. The SOC-induced breaking of the band degeneracy points between the valence and conduction bands is clearly observed by ARPES. However, the strength of SOC is found to be insufficient to open a band gap, which makes monolayer 1T'-$MoTe_2$ on bilayer graphene a semimetal.

Two-dimensional (2D) transition metal dichalcogenide (TMDC) is a versatile material platform, in which electrical, optical, and topological properties can be controlled through thickness, strain, field, and other perturbations.[1, 2, 3, 4] The most well-studied example is 2H-MX_2 (M=Mo, W; X=S, Se) semiconductor that makes a transition from indirect band gap to direct band gap only in the monolayer[4 5], with well-pronounced spin-splitting[6, 7] and valley degrees of freedom[8, 9]. Other structural phases stemming from different stacking orders between transitional metal and chalcogen layers deliver distinct physical properties even with the same constituent atoms.

1T'-MX_2 (M=Mo, W; X=S, Se, Te) has gained particular interest regarding its topological properties. While its three-dimensional bulk form has been explored in terms of type-II Weyl semimetal[10, 11, 12, 13], the monolayer is predicted to host quantum spin Hall (QSH) insulator[3]. QSH insulator, or two-dimensional (2D) topological insulator, is a topologically nontrivial quantum state, which is hallmarked by the helical edge state protected by time reversal symmetry and the bulk (as opposed to the edge) band gap opening due to strong spin-orbit coupling (SOC)[14, 15, 16]. The resulting transport properties exhibit quantized Hall conductance even in the absence of magnetic field, and spin-polarized edge current are expected to be useful for the spintronic applications. The QSH phase in 1T' TMDC has been recently realized only in 1T'-WTe_2[17, 18]. It is of great interest whether it is possible to realize a QSH state in other 1T' TMDCs and whether fundamental parameters such as bulk band gap would be different from those of 1T'-WTe_2.

Many efforts have been devoted to achieve a QSH state in monolayer 1T'-$MoTe_2$.[3,

[19, 20, 21] From the electronic structure point of view, two critical elements of achieving a QSH state in group VI TMDCs are the band inversion caused by the structural distortion from 1T phase to 1T' and the 2D bulk band gap induced by strong SOC.[18] The former has been well established by the previous theoretical calculations. [3, 19, 20] However, as shown in Table 1, the calculated band gap size varies significantly depending on calculation methods, even to a degree that it is not clear whether 1T'-$MoTe_2$ is a semiconductor or a semimetal. Optical absorption and transport measurements report a 60 meV bulk gap in few layer mechanically exfoliated (ME) 1T'-$MoTe_2$,[20] while CVD-grown monolayer 1T'-$MoTe_2$ shows a metallic transport behavior.[21] Whether the SOC is strong enough to open a bulk gap is still not very clear. A characterization tool that can directly visualize the band structure and the size of the band gap, such as angle-resolved photoemission spectroscopy (ARPES)[22, 23], would provide a clearer insight on this aspect.

In this Letter, we report a successful growth of monolayer 1T'-$MoTe_2$ on bilayer graphene (BLG) substrate using molecular beam epitaxy (MBE). The electronic structure of epitaxial 1T'-$MoTe_2$ has been investigated by in-situ ARPES. We found that the SOC indeed breaks the band degeneracy points and separates the valence and conduction bands. However, the strength of SOC is not enough to open a 2D bulk band gap, which makes monolayer 1T'-$MoTe_2$ on BLG a semimetal.

Both thin film growth and ARPES characterization of 1T'-$MoTe_2$ were performed at the Beamline 10.0.1, Advanced Light Source, Lawrence Berkeley National Laboratory. 1T'-$MoTe_2$ was grown by MBE with a base pressure of ~2×10^{-10} Torr. Mo

(99.99% purity) and Te (99.999% purity) were evaporated by an e-beam evaporator and a Knudsen cell, respectively, with the flux ratio of ~ 1:20. The substrate was BLG prepared by vacuum graphitization of 6H-SiC(0001).[24] The substrate temperature was set at 280^{O}C for growth. The flux ratio between Mo and Te was 1:10. The growth rate was 15 minutes per layer. Following the growth, a 20-minute post annealing process at the same temperature was performed. Additional ARPES measurements were performed at the Beamline 5-4, Stanford Synchrotron Radiation Lightsource (SSRL), SLAC National Accelerator Laboratory. The band structure calculation is performed by using generalized gradient approximation method with PBE exchange-correlation functional as implemented in the VASP package[25]. The lattice constant used is of a = 6.38 Å, b = 3.45 Å for 1T'-$MoTe_2$.

The crystal structure of 1T'-$MoTe_2$ is illustrated in Fig. 1a. It can be seen as a distorted 1T-$MoTe_2$, for which Mo atoms are in octahedral coordination with Te atoms. With the distortion, Mo atoms shift off the center of Te octahedra toward X direction forming zigzag metal chains along Y direction. The Te atoms also shift accordingly, making two types of Te with inequivalent coordinations. Fig. 1b shows the Brillion zone of 1T'-$MoTe_2$. The Reflection high-energy electron diffraction (RHEED) patterns before and after the thin film growth are shown in Fig. 1c. The sharp diffraction stripes after growth indicate the high crystalline quality of 1T'-$MoTe_2$ thin film. The thermal stability of the sample is checked by annealing the sample at 350 ^{O}C under Te atmosphere. No obvious change in RHEED pattern was observed, indicating growth temperature 280 ^{O}C is far below the decomposing temperature, thus retaining high

crystallinity of the sample[26]. Using lattice constant of BLG ~ 2.46 Å as a reference, one can get the lattice parameter of 1T'-$MoTe_2$ on BLG ~ 6.3 Å, which is consistent with reported values[3]. Fig. 1d is the angle-integrated core level spectrum, clearly showing the characteristic Mo 4*p* peak and Te 4*d* peaks. Figure 2 is the low-energy electron diffraction (LEED) pattern taken with electron kinetic energy of 94 eV to reveal the surface symmetry and lattice structure. The blue solid circles indicate the first-order diffraction from BLG substrate. The six spots surrounding each of them come from $6\sqrt{3}$R30° superlattice diffractions between graphene and SiC[24]. Due to the symmetry mismatch between three-fold rotational symmetric BLG and two-fold symmetric 1T'-$MoTe_2$, there are three energetically equivalent rotational alignments between BLG and 1T'-$MoTe_2$[27]. This results in three sets of reciprocal lattices superposed in both LEED and ARPES data. The LEED pattern from different domains of 1T'-$MoTe_2$ are indicated by the dotted lines with different colors in Fig. 2a. Using the in-plane lattice constant of graphene a = 2.46Å, one can get the lattice constant of 1T'-$MoTe_2$, a = 6.3 Å, b = 3.4 Å, consistent with the previously reported values[3] as well as with that from our RHEED measurement. Fig. 2b shows the superposition of the Brillion zones from three equivalent 1T'-$MoTe_2$ and graphene lattices.

Figure 3 show the overall electronic structure and Fermi surface (FS) topology from ARPES measurements on the monolayer 1T'-$MoTe_2$/BLG. Fig. 3a is the FS intensity map, which shows six-fold symmetry due to the superposition of three 1T'-$MoTe_2$ domains with 120° rotation with respect to each other. One may extract single-domain FS from the ARPES data as shown in Fig. 3b. There are one hole pocket located at the

zone center, two electron pockets along the ΓY direction, and two more electron pockets located at the zone boundaries. The topology of the FS plays a key role in understanding the transport properties of the semimetal in which the hole and electron carriers coexist. Perfect electron-hole compensation is proposed to be responsible for the non-saturating magneto-resistance in three-dimensional bulk 1T'-WTe_2.[28] However, too many bands crossing the Fermi energy (E_F) in a confined momentum space have challenged ARPES measurements and interpretations.[29, 30] The simplified FS in monolayer 1T'-$MoTe_2$ makes the evaluation easier and reliable. We have obtained concentration ratio between the *n* and *p* type carriers ~ 6:10. Considering that the volume of electron (hole) pocket increase (decrease) very quickly above the E_F, one may easily achieve the *n* and *p* carries balance with slightly doping on the film to realize the electron-hole compensation condition in the monolayer[1, 31].

Fig. 3c is the overall band structure along the ΓY direction measured by in-situ ARPES, superimposed with the theoretical calculation made with PBE method. Due to the superimposed rotational domains, the signal from the ΓP direction (Fig. 1b) overlaps with that from ΓY direction within a single detection plane. However, the low energy bands from ΓP are contained within the envelop of ΓY bands in both theory and experiment. The domain size of the film is estimated to be tens of nanometer[1, 18], which call for further studies with characterization tools with high spatial resolution such as STM and nano-ARPES to disentangle the superposition of signals from domains with different orientations. Overall, the experimental band structure and FS topology from ARPES agree well with the theoretical calculation.

Now we focus on the low energy electronic structure right near the E_F. According to theoretical calculations,[3, 19, 20] the transition from 1T to 1T' inverts the band order leading to a band degeneracy point between the valence and conduction band at Δ point (Fig. 4a, left). The SOC then lift the degeneracy at the cross point (Fig 4b, right) to make the system to be an insulator with a bulk band gap or a semimetal, depending on the strength of the coupling. The low energy band dispersion along both ΓX and ΓY directions (Fig. 4b and c), and corresponding momentum distribution curves (MDCs) and energy distribution curves (EDCs) along the ΓY direction (Fig.4 d and e) clearly indicate well-separated valence and conduction bands confirming the scenario mentioned above. The relatively broad linewidth of EDCs may indicate the possible variation of the gap size from domain to domain due to the much larger ARPES beam spot size than the typical domain size of the sample. Nonetheless, the band structure measured by ARPES clearly exhibit that the hole band at Γ crosses the E_F, while the conduction band minimum locates well below the E_F, leading to a FS with both electron and hole pockets. This shows that monolayer 1T'-$MoTe_2$ on BLG is a semimetal with a moderate strength of SOC.

Considering the weaker SOC in Mo compared to W, in general, one would expect that the SOC-induced energy bandgap in 1T'-$MoTe_2$ is smaller than that in 1T'-WTe_2. In addition, strain and electron-electron interaction are believed to play important roles in the low energy electronic structure of 1T'-$MoTe_2$.[3, 32] As shown in the calculations[3,32], size of the gap is very sensitive to the lattice constant. However, a large strain, ~ 4~6% of the lattice constant, is needed to lift the crossover of conduction and valence band

and to open the bulk gap. It has been known that van der Waals epitaxy adopted in our growth of 1T'-$MoTe_2$ on graphene minimize the strain effect caused by lattice mismatch[33]. A strong electron-electron correlation, which is largely screened in the bulk 1T'-$MoTe_2$, could also enlarge the separation between the conduction and the valence band[32]. As calculated in Ref. 32, even with a very strong on-site Coulomb repulsion ~ 5 eV, the band gap remains closed for 1T'-$MoTe_2$. In our 1T'-$MoTe_2$/BLG thin films, the conducting graphene substrate enhances the screening to lower the strength of on-site Coulomb interactions, which would act against the bulk gap opening due to the electron-electron interaction.

In summary, high-quality monolayer 1T'-$MoTe_2$ has been grown on BLG substrate by MBE. In-situ LEED and ARPES measurements are performed to characterize the crystal and electronic structure. It has been shown that three equivalent rotational domains of 1T'-$MoTe_2$ coexist and contribute to our spectra. The overall electronic structure obtained from ARPES exhibit excellent agreement with theoretical calculations, including the predicted degeneracy lifting induced by SOC. However, the splitting due to the SOC is not large enough to open a 2D bulk gap. The valence band maximum locates above the conduction band minimum resulting in a FS with both electron and hole pockets. Our measurements confirm that the epitaxially-grown monolayer 1T'-$MoTe_2$ on BLG is a semimetal.

Acknowledgments

The ARPES and thin film growth works at the Stanford Institute for Materials and

Energy Sciences and Stanford University are supported by the Office of Basic Energy Sciences, Division of Materials Science and AFOSR Grant FA9550-14-1-0277 through the University of Washington that support the ALS activity by the Stanford team. Research performed at ALS (thin film growth and ARPES) is supported by the Office of Basic Energy Sciences, US DOE under Contract No. DE-AC02-05CH11231. SSRL is supported by the Office of Basic Energy Sciences, US DOE under Contract No. DE-AC02-76SF00515. Z. L. is supported by the National Natural Science Foundation of China (11227902). S. T. acknowledges the support by CPSF-CAS Joint Foundation for Excellent Postdoctoral Fellows. H. R. and C. H. acknowledge the support from the NRF, Korea through Max Planck Korea/POSTECH Research Initiative (No. 2011-0031558) and Basic Science Research Program (No. 2015R1C1A1A01053065). A portion of the computational work was performed using the resources of the National Energy Research Scientific Computing Center (NERSC) supported by the US Department of Energy, Office of Science, under Contract No. DE-AC02-05CH11231.

References

1. Zhang Y, Chang T-R, Zhou B, Cui Y-T, Yan H, Liu Z, Schmitt F, Lee J, Moore R, Chen Y, Lin H, Jeng H-T, Mo S-K, Hussain Z, Bansil A, Shen Z-X. Direct observation of the transition from indirect to direct bandgap in atomically thin epitaxial $MoSe_2$. *Nat Nanotech* 2014, **9**(2)**:** 111-115.

2. Desai SB, Seol G, Kang JS, Fang H, Battaglia C, Kapadia R, Ager JW, Guo J, Javey A. Strain-Induced Indirect to Direct Bandgap Transition in Multilayer WSe_2. *Nano Lett* 2014, **14**(8)**:** 4592-4597.

3. Qian X, Liu J, Fu L, Li J. Quantum spin Hall effect in two-dimensional transition metal dichalcogenides. *Science* 2014, **346**(6215)**:** 1344-1347.

4. Mak KF, Lee C, Hone J, Shan J, Heinz TF. Atomically Thin MoS_2: A New Direct-Gap Semiconductor. *Phys Rev Lett* 2010, **105**(13)**:** 136805.

5. Splendiani A, Sun L, Zhang Y, Li T, Kim J, Chim C-Y, Galli G, Wang F. Emerging Photoluminescence in Monolayer MoS_2. *Nano Lett* 2010, **10**(4)**:** 1271-1275.

6. Riley JM, Mazzola F, Dendzik M, Michiardi M, Takayama T, Bawden L, Granerod C, Leandersson M, Balasubramanian T, Hoesch M, Kim TK, Takagi H, Meevasana W, Hofmann P, Bahramy MS, Wells JW, King PDC. Direct observation of spin-polarized bulk bands in an inversion-symmetric semiconductor. *Nat Phys* 2014, **10**(11)**:** 835-839.

7. Mo S-K, Hwang C, Zhang Y, Fanciulli M, Muff S, Dil JH, Shen Z-X, Hussain Z. Spin-resolved photoemission study of epitaxially grown $MoSe_2$ and WSe_2 thin films. *J Phys Condens Matter* 2016, **28**(45)**:** 454001.

8. Mak KF, He K, Shan J, Heinz TF. Control of valley polarization in monolayer MoS_2 by optical helicity. *Nat Nanotech* 2012, **7**(8)**:** 494-498.

9. Mak KF, McGill KL, Park J, McEuen PL. The valley Hall effect in MoS_2 transistors. *Science* 2014, **344**(6191)**:** 1489-1492.

10. Deng K, Wan G, Deng P, Zhang K, Ding S, Wang E, Yan M, Huang H, Zhang H, Xu Z, Denlinger J, Fedorov A, Yang H, Duan W, Yao H, Wu Y, Fan S, Zhang H, Chen X, Zhou S. Experimental observation of topological Fermi arcs in type-II Weyl semimetal $MoTe_2$. *Nat Phys* 2016, **12**(12)**:** 1105-1110.

11. Tamai A, Wu QS, Cucchi I, Bruno FY, Riccò S, Kim TK, Hoesch M, Barreteau C, Giannini E, Besnard C, Soluyanov AA, Baumberger F. Fermi Arcs and Their Topological Character in the Candidate Type-II Weyl Semimetal $MoTe_2$. *Phy Rev X* 2016, **6**(3)**:** 031021.

12. Sun Y, Wu S-C, Ali MN, Felser C, Yan B. Prediction of Weyl semimetal in orthorhombic $MoTe_2$. *Phys Rev B* 2015, **92**(16)**:** 161107.

13. Jiang J, Liu ZK, Sun Y, Yang HF, Rajamathi CR, Qi YP, Yang LX, Chen C, Peng H, Hwang CC, Sun SZ, Mo SK, Vobornik I, Fujii J, Parkin SSP, Felser C, Yan BH, Chen YL. Signature of type-II Weyl semimetal phase in $MoTe_2$. *Nature communication* 2017, **8:** 13973.

14. Murakami S. Quantum Spin Hall Effect and Enhanced Magnetic Response by Spin-Orbit Coupling. *Phys Rev Lett* 2006, **97**(23)**:** 236805.

15. Bernevig BA, Hughes TL, Zhang S-C. Quantum Spin Hall Effect and Topological Phase Transition in HgTe Quantum Wells. *Science* 2006, **314**(5806)**:** 1757-1761.

16. Kane CL, Mele EJ. Quantum Spin Hall Effect in Graphene. *Phys Rev Lett* 2005, **95**(22)**:** 226801.

17. Fei Z, Palomaki T, Wu S, Zhao W, Cai X, Sun B, Nguyen P, Finney J, Xu X, Cobden DH. Edge conduction in monolayer WTe_2. *Nat Phys* 2017, **13**(7)**:** 677-682.

18. Tang S, Zhang C, Wong D, Pedramrazi Z, Tsai H-Z, Jia C, Moritz B, Claassen M, Ryu H, Kahn S, Jiang J, Yan H, Hashimoto M, Lu D, Moore RG, Hwang C-C, Hwang C, Hussain Z, Chen Y, Ugeda MM, Liu Z, Xie X, Devereaux TP, Crommie MF, Mo S-K, Shen Z-X. Quantum spin Hall state in monolayer 1T'-WTe_2. *Nat Phys* 2017, **13**(7)**:** 683-687.

19. Choe D-H, Sung H-J, Chang KJ. Understanding topological phase transition in monolayer transition metal dichalcogenides. *Phys Rev B* 2016, **93**(12)**:** 125109.

20. Keum DH, Cho S, Kim JH, Choe D-H, Sung H-J, Kan M, Kang H, Hwang J-Y, Kim SW, Yang H, Chang KJ, Lee YH. Bandgap opening in few-layered monoclinic $MoTe_2$. *Nat Phys* 2015, **11**(6)**:** 482-486.

21. Naylor CH, Parkin WM, Ping J, Gao Z, Zhou YR, Kim Y, Streller F, Carpick RW, Rappe AM, Drndić M, Kikkawa JM, Johnson ATC. Monolayer Single-Crystal 1T′-$MoTe_2$ Grown by Chemical Vapor Deposition Exhibits Weak Antilocalization Effect. *Nano Lett* 2016, **16**(7)**:** 4297-4304.

22. Damascelli A, Hussain Z, Shen Z-X. Angle-resolved photoemission studies of the cuprate superconductors. *Rev Mod Phys* 2003, **75**(2)**:** 473-541.

23. Mo S-K. Angle-resolved photoemission spectroscopy for the study of two-dimensional materials. *Nano Convergence* 2017, **4**(1)**:** 6.

24. Qingyan W, Wenhao Z, Lili W, Ke H, Xucun M, Qikun X. Large-scale uniform bilayer graphene prepared by vacuum graphitization of 6H-SiC(0001) substrates. *J Phys Condens Matter* 2013, **25**(9)**:** 095002.

25. Kresse G, Furthmüller J. Efficient iterative schemes for ab initio total-energy calculations using a plane-wave basis set. *Phys Rev B* 1996, **54**(16)**:** 11169-11186.

26. Choi BK, Kim M, Jung K-H, Kim J, Yu K-S, Chang YJ. Temperature dependence of band gap in MoSe2 grown by molecular beam epitaxy. *Nanoscale Research Letters* 2017, **12**(1)**:** 492.

27. Wang E, Ding H, Fedorov AV, Yao W, Li Z, Lv Y-F, Zhao K, Zhang L-G, Xu Z, Schneeloch J, Zhong R, Ji S-H, Wang L, He K, Ma X, Gu G, Yao H, Xue Q-K, Chen X, Zhou S. Fully gapped topological surface states in Bi_2Se_3 films induced by a d-wave high-temperature superconductor. *Nat Phys* 2013, **9**(10)**:** 621-625.

28. Ali MN, Xiong J, Flynn S, Tao J, Gibson QD, Schoop LM, Liang T, Haldolaarachchige N, Hirschberger M, Ong NP, Cava RJ. Large, non-saturating magnetoresistance in WTe_2. *Nature* 2014, **514**(7521)**:** 205-208.

29. Thirupathaiah S, Jha R, Pal B, Matias JS, Das PK, Sivakumar PK, Vobornik I, Plumb NC, Shi M, Ribeiro RA, Sarma DD. $MoTe_2$: An uncompensated semimetal with extremely large magnetoresistance. *Phys Rev B* 2017, **95**(24)**:** 241105.

30. Chen-Lu W, Yan Z, Jian-Wei H, Guo-Dong L, Ai-Ji L, Yu-Xiao Z, Bing S, Jing L, Cheng H, Ying D, De-Fa L, Yong H, Shao-Long H, Lin Z, Li Y, Jin H, Jiang W, Zhi-Qiang M, You-Guo S, Xiao-Wen J, Feng-Feng Z, Shen-Jin Z, Feng Y, Zhi-Min W, Qin-Jun P, Zu-Yan X, Chuang-Tian C, Xing-Jiang Z. Evidence of Electron-Hole Imbalance in WTe_2 from High-Resolution Angle-Resolved Photoemission Spectroscopy. *Chinese Physics Letters* 2017, **34**(9)**:** 097305.

31. Kang M, Kim B, Ryu SH, Jung SW, Kim J, Moreschini L, Jozwiak C, Rotenberg E, Bostwick A, Kim KS. Universal Mechanism of Band-Gap Engineering in Transition-Metal Dichalcogenides. *Nano Lett* 2017, **17**(3)**:** 1610-1615.

32. Kim H-J, Kang S-H, Hamada I, Son Y-W. Origins of the structural phase transitions in $MoTe_2$ and WTe_2. *Phys Rev B* 2017, **95**(18)**:** 180101.

33. Novoselov KS, Mishchenko A, Carvalho A, Castro Neto AH. 2D materials and van der Waals heterostructures. *Science* 2016, **353**(6298).

Table1. Gap size derived from different calculation methods and experimental measurements

Calculation or experiment method	Sample fabrication method & thickness	Gap size (eV)	Bulk Conductivity	reference
PBE	--	-0.262	Metallic	Ref. 3
G_0W_0	--	-0.300	Metallic	Ref. 3
PBE+HSE06	--	0.03	semiconductor	Ref. 20
transport	CVD monolayer	--	Metallic	Ref. 21
Optical absorption	ME few layer	0.06	semiconductor	Ref. 20
ARPES	MBE monolayer	--	Metallic	This work

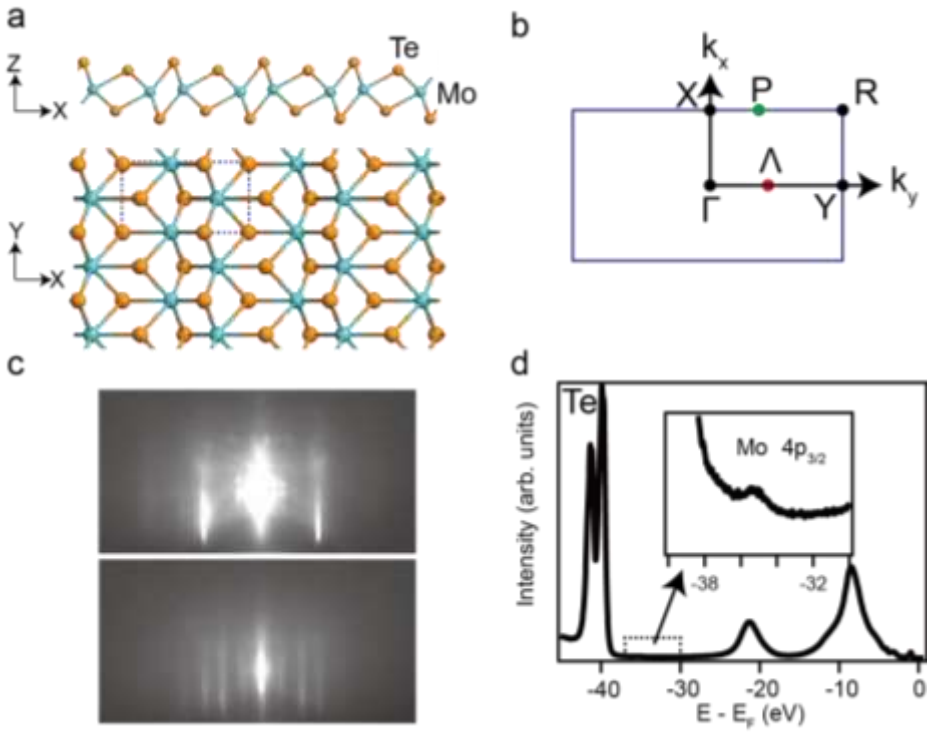

Fig. 1. MBE growth of 1T'-$MoTe_2$ (a) Crystal structure of 1T'-$MoTe_2$, side view (upper panel) and top view (lower panel). (b) Brillouin Zone of 1T'-$MoTe_2$. (c) RHEED patterns of graphene substrate (top) and after monolayer 1T'-$MoTe_2$ film growth (bottom). (d) Core level spectrum of 1T'-$MoTe_2$ thin film, the inset is the zoom-in of the boxed part.

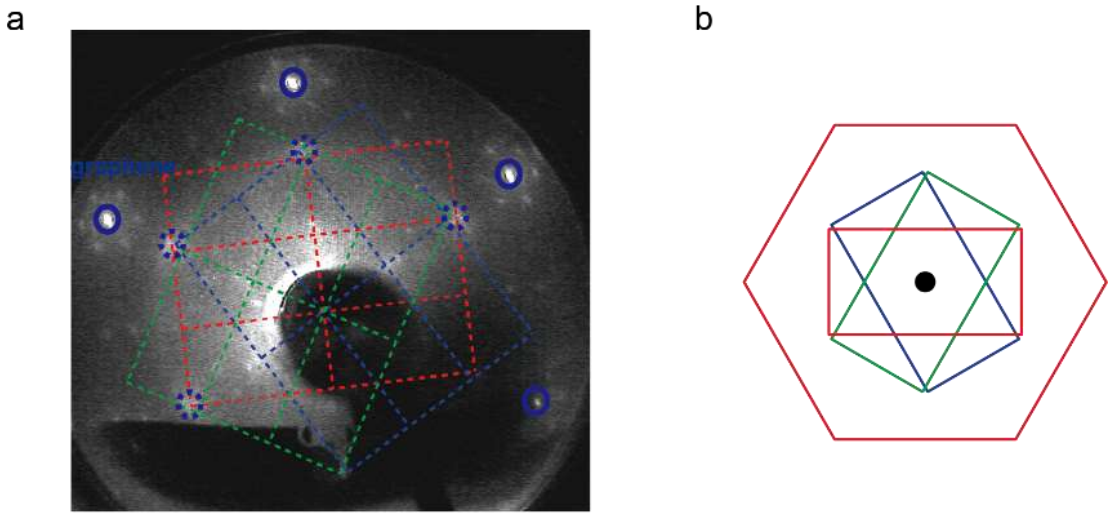

Fig. 2. LEED pattern of 1T'-$MoTe_2$ film. (a) LEED pattern (94 eV) of the film. Blue solid circles are the first-order reflection from graphene. The blue dotted circles indicate the reflections from 1T'-$MoTe_2$. (b) Superposition of the Brillion zones of 1T'-$MoTe_2$ (blue, green, and red rectangles) and BLG (red hexagon).

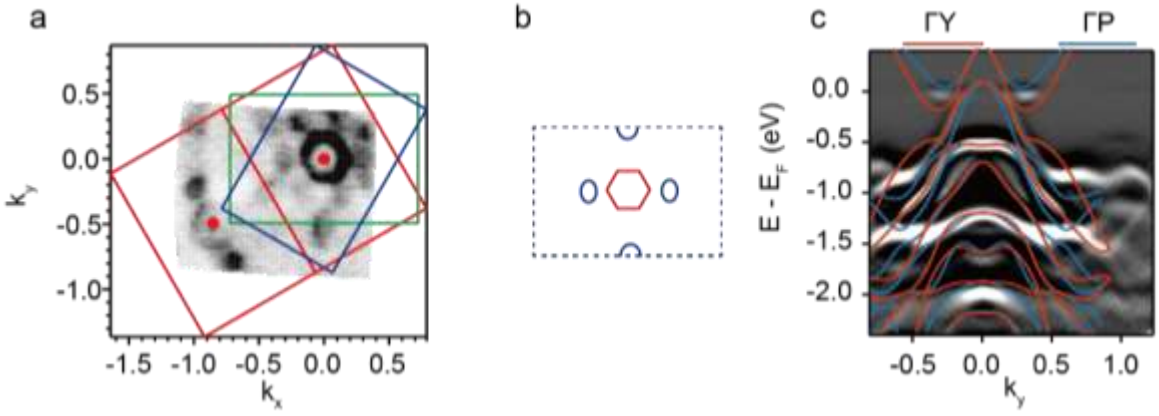

Fig. 3. Electronic structure of monolayer 1T'-$MoTe_2$. (a) Fermi surface intensity map from ARPES measurement of monolayer 1T'-$MoTe_2$. The intensity is integrated within a $\pm$10 meV window around the Fermi energy. The red, blue and green rectangles indicate three Brillion Zones from three rotational domains, 120 degrees with respect to each other. (b) Fermi surface topology extracted from ARPES data for a single domain. The red and blue pockets represent the hole and electron pockets, respectively. (c) The second derivative of ARPES spectrum along ΓY superposed with PBE calculation. The red and blue lines are calculated bands along the ΓY and ΓP directions, respectively.

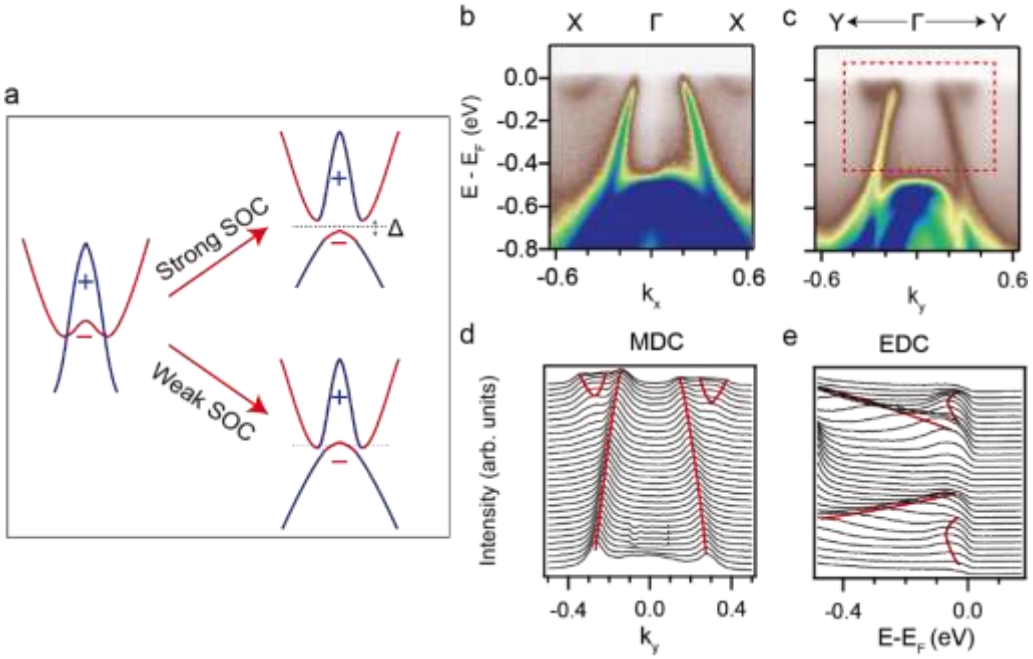

Fig. 4. Detailed view of low-energy electronic structure of monolayer 1T'-$MoTe_2$. (a) The band evolution of 1T'-TMDCs under strong and weak SOC. (b, c) Detailed ARPES spectra along the ΓX and ΓY directions, respectively. (d, e) MDCs and EDCs along the ΓY direction corresponding to the boxed area in c.

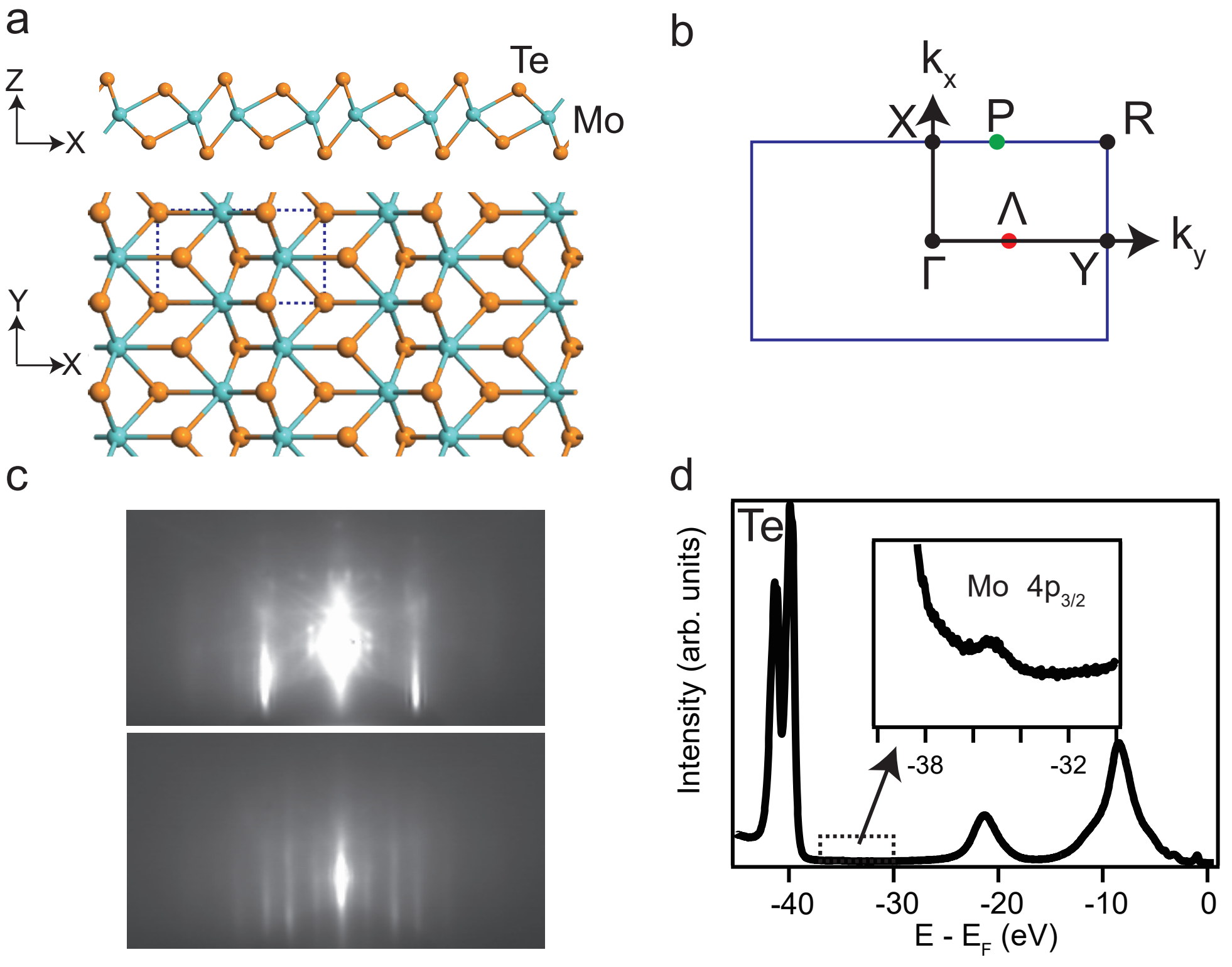
a
z
x
Te
Mo
Y
x
b
k_x
X
P
R
Λ
Γ
Y
k_y
c
d
Te
Mo 4p$_{3/2}$
-38
-32
Intensity (arb. units)
-40
-30
-20
-10
0
E - E$_F$ (eV)

a

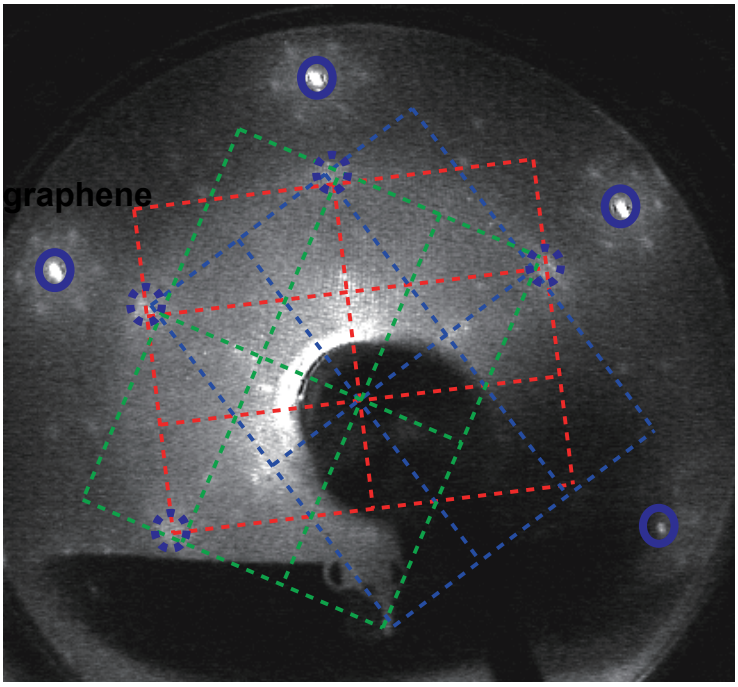

b

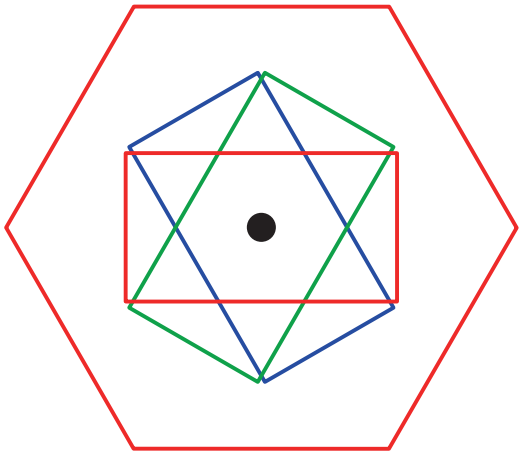

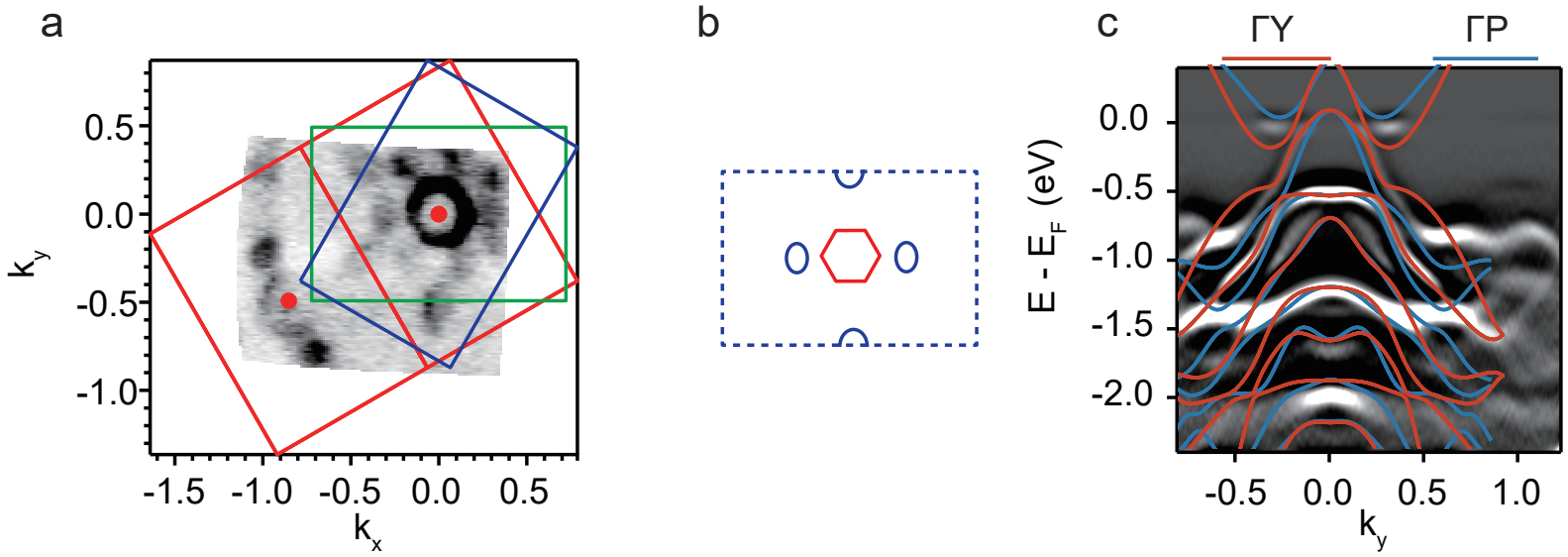
a
b
c
ΓY
ΓP
0.5
0.0
-0.5
-1.0
k_y
-1.5
-1.0
-0.5
0.0
0.5
k_x
$E - E_F$ (eV)
0.0
-0.5
-1.0
-1.5
-2.0
-0.5
0.0
0.5
1.0
k_y

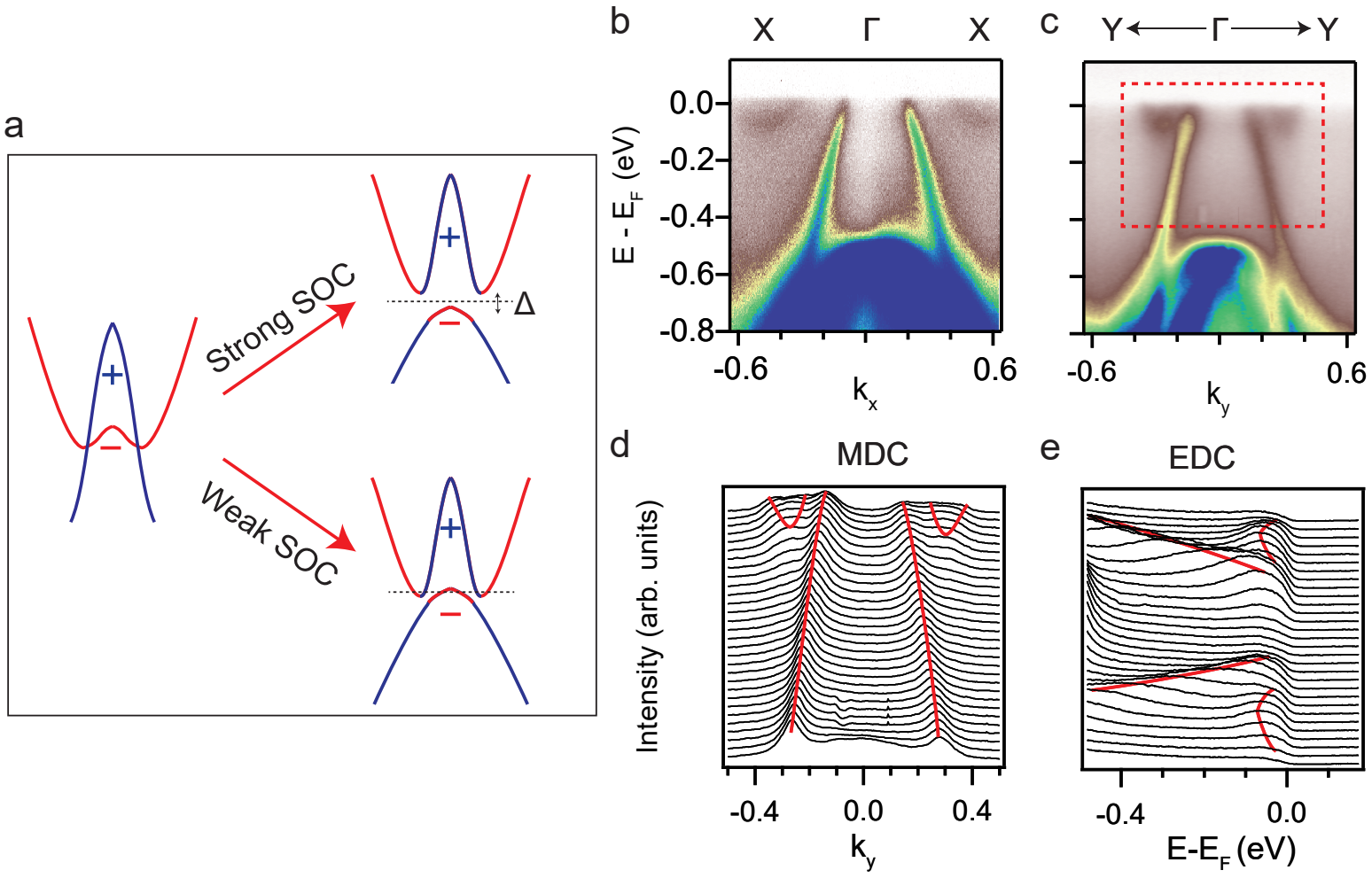
a
Strong SOC
Weak SOC
+
−
Δ
b
X
Γ
X
0.0
-0.2
-0.4
-0.6
-0.8
E - E_F (eV)
-0.6
0.6
k_x
c
Y
Γ
Y
-0.6
0.6
k_y
d
MDC
Intensity (arb. units)
-0.4
0.0
0.4
k_y
e
EDC
-0.4
0.0
E-E_F (eV)